Kinetics of surface steps in the presence of impurities: Patterns and instabilities

Daniel Kandel*
Institute for Physical Science and Technology, University of Maryland, College Park, Maryland 20742

John D. Weeks
Institute for Physical Science and Technology, University of Maryland, College Park, Maryland 20742
and Department of Chemistry, University of Maryland, College Park, Maryland 20742
(Received 23 November 1994)

We consider the flow of atomic steps on a crystal surface in the presence of impurities. A mesoscopic model of the effect is proposed and studied by numerical simulations. In the small line tension limit complex highly connected step patterns are formed that exhibit distinct repeating features. To explain these features we make the ansatz that the system is locally close to weakly unstable steady states. Using a differential equation approach we calculate these steady-state configurations analytically, and verify the ansatz; the analytical predictions are in agreement with numerical simulations. We also predict that the typical length scale of the patterns should grow with time as $\sqrt{t}$. This coarsening law is consistent with numerical simulations of the mesoscopic model.

I. INTRODUCTION

One of the most important modes of crystal growth is the *step flow* mode.[1] In this regime, crystal growth (or evaporation) occurs predominantly by the motion of fairly straight and uniformly spaced atomic steps, produced say, by cutting the crystal surface at a small angle to a close packed plane. Conditions are such that the formation of islands on the terraces between the steps can be neglected. Crystal growth in the step flow mode can be controlled very accurately and yields high-quality crystals. As an example for the degree of control one can achieve, let us mention the use of stepped surfaces as substrates in the fabrication of nanostructures such as quantum wires.[2]

The uniformity of the step train is essential for the growth of crystals of high quality. Under some experimental conditions, however, this uniformity is lost due to kinetic instabilities, which lead to bending as well as bunching of the steps.[3] Several different mechanisms have been proposed as causes for these instabilities.[4,5] We concentrate here on an important general mechanism proposed by Frank.[6] He advanced the idea that impurities in the flux of atoms impinging on the surface during crystal growth may lead to a step bunching instability. Different aspects of the impurity mechanism have been further investigated by other researchers.[7,8] Recently, we studied[9] the long time dynamics of a step train, subject to a flux of impurities, using a mesoscopic model of step flow, in the large line tension limit. In the present paper we investigate in detail the interesting behavior of this model in the small line tension limit where step bending becomes significant. A partial account of this work is given in Ref. 10.

The paper is organized as follows. In the remainder of the Introduction we give an intuitive explanation of Frank's impurity mechanism. In the next section we describe our mesoscopic model for step flow and present results of simulations of the model. A differential equation approach to the problem is developed in Sec. III. Analytical steady-state solutions of the set of differential equations are presented in Secs. IV, VI, and VII. In Sec. V, we compare numerical solutions of the differential equations to step patterns obtained from simulations of the mesoscopic model. The coarsening kinetics associated with the step bunching process is discussed in Sec. VIII.

Standard approaches like the Burton, Cabrera, and Frank (BCF) theory[1] describe processes such as atom exchange between steps and terraces, surface diffusion, and adatom attachment and detachment from terraces using a set of differential equations with appropriate boundary conditions on the step edges. When steps are straight, these can be replaced by equations giving the velocity of each step as a function of the widths of the terraces in front (i.e., in the direction of step motion) and behind it. We will consider the consequences of such a description for step bunching assuming only very general properties of the velocity functions. Because of the increased area available for adatom exchange between the terraces and the vapor, we expect that the step velocity will be an increasing function of the terrace widths for widths less than some characteristic surface diffusion distance. Stable step flow results when the contribution from the terrace in front is most important,[8,11] and we assume that is the case here. (We have recently studied the opposite case[12] where the contribution from the terrace behind dominates.)

Frank argued that a small flux of certain kinds of impurities impinging on the surface during crystal growth (or evaporation) could destabilize the uniform step train. The impurities Frank envisioned have the following essential properties: (i) They impede the motion of steps. When an impurity is present immediately in front of a portion of a step, the velocity of that portion is reduced

compared to its velocity in the absence of an impurity. (ii) Once an impurity is passed by a step it is *deactivated* (i.e., covered or buried during growth or removed from the surface during evaporation) and ceases to affect subsequent step motion.

We showed in a previous publication[9] that when the impurities are not too strong, one can write down a set of coupled equations describing the motion of the steps:[11]

$$\frac{dX_n}{dt} = f(W_n), \tag{1}$$

where X_n is the position of step n and $W_n \equiv X_{n+1} - X_n$ is the width of the terrace in front of it. (The step index n increases in the direction of step motion.) At small W, the impurity density is small [from property (ii)] and f should *increase* with W, just as is the case without impurities. However, when W_n is large and the density of impurities C_n is high, the impurity effect in (i) dominates and the step velocity $f(W)$ should be a *decreasing* function of W. Finally, since step crossings are forbidden because of the high energy cost of overhangs, we require f to vanish when $W \to 0$. We conclude that $f(W)$ increases from zero for small W, reaches a maximum at some value $W = W^m$, and decreases as W increases for $W > W^m$. Note that a velocity function f of this type allows steps to bunch together but not to cross. It is easy to see[9] that the use of such an f in (1) causes the uniform step train with all $W_n = W^0 > W^m$ to be linearly unstable toward *step pairing*. Similarly the uniform step train is linearly stable when $W^0 < W^m$.

Before performing a detailed investigation of the consequences of this instability, let us comment on the generality of Frank's impurity mechanism. First of all, although Frank described it for crystal growth, it is equally relevant for crystal evaporation, and indeed our mathematical description of the dynamics [see, e.g., Eq. (1)] does not distinguish between growth and evaporation. Second, the impurity concept is much more general than one might at first think. In Ref. 9 we argued that *generalized impurities* generated by the step flow process itself (without the need for an external flux of impurities), may have the properties of Frank's impurities (see above), and can thus generate a similar instability. Finally, our analysis of the instability is valid for any mechanism that leads to a step flow description in terms of a velocity function with the properties of the function f defined above (even if the mechanism does not involve impurities of any kind).

II. A MESOSCOPIC MODEL FOR THE FRANK INSTABILITY

Since steps need not remain straight during the bunching process, the above picture should be extended to two dimensions. In principle, we should model both adatom diffusion and the behavior of impurities on a microscopic level in order to obtain an accurate description of the Frank instability. From the point of view of numerical calculations this is unrealistic, since we are interested in the long time behavior of a fairly large system. Since adatom diffusion is relatively well understood and is not the source of instabilities here, it can be taken into account in an averaged way by using a velocity function f_0 that is an increasing function of the local terrace width. The collective effect of impurities, on the other hand, is not so well known; indeed, this is the main subject of investigation of this work. In particular, our model[9] will take account of the fact that the local adsorption of impurities is inherently a two-dimensional time-dependent process.

Consider a system of N steps each consisting of L vertical segments that reside on the links of a square lattice. There is a "line tension" interaction between nearest neighbor segments of the same step:

$$E = \gamma \sum_{n,y} [X_n(y+1) - X_n(y)]^2 , \tag{2}$$

where $X_n(y)$ is the position of the yth segment of the nth step, and γ is the effective line tension. This term favors straight steps at low temperatures.

In the absence of impurities, we use the following rules for step motion.

(1) Select a step segment at random, say segment y of step n.

(2) Attempt to move it backwards with probability $p_b = (1 - A)/2$, or forward with probability $p_f = p_b + A\{1 - \exp[-W_n(y)/l_d]\}$. Here $W_n(y) \equiv X_{n+1}(y) - X_n(y)$ is the local terrace width, l_d is the main component diffusion length, and A is a monotonically increasing function of the flux of main component atoms, which vanishes when the flux is equal to the equilibrium flux.

(3) Always reject the attempted move if it leads to terraces of width smaller than 1. (This corresponds to overhanging steps.) If this no-overhang condition is not violated, reject the move with probability $1 - \exp(-\beta \Delta E)$ if it raises the line tension energy by an amount ΔE, and accept it otherwise. Here β is the inverse temperature.

At equilibrium, with $A = 0$, these rules reproduce the usual Monte Carlo kinetics of steps, where fluctuations (whose magnitude is controlled by a line tension) generate an entropic repulsive interaction.

Now consider the adsorption of impurities with the properties (i) and (ii) of Frank's model.[6,9] Such impurities arrive at random vacant sites of the lattice and for simplicity do not diffuse. (Multiple occupancy is prohibited.) When attempting to move a step segment forward past an impurity, the acceptance probability of the move is reduced by a factor $0 < 1 - S < 1$ compared to the probability in the absence of an impurity [rule (3) above]. If the move is accepted, the impurity is deactivated and no longer affects step motion. The microscopic parameter S is associated with the strength of impurities. If $S \approx 0$ the impurities are weak, whereas $S \approx 1$ is the strong impurity limit.

We simulate the model in the following way. Starting with uniformly spaced straight steps and a surface free of impurities, we perform successive sweeps of impurity deposition and step flow. In an impurity deposition sweep, we pick at random $F_i N L W^0$ sites, where F_i is the flux of impurities and W^0 is the initial terrace width. Impurities are deposited in all the selected *vacant* sites. Each

step flow sweep consists of NL attempts to move step segments chosen at random. The attempts are done according to rules (1)–(3) above, taking into account the effects of impurities on step motion as well.

A few comments about the model are now in order. It is not a microscopic model since adatom diffusion is taken into account only effectively through the use of a velocity function for the steps in the absence of impurities [rule (2) above]. This is fairly satisfactory under most conditions, but completely excludes diffusional instabilities of the Mullins-Sekerka type.[5] Moreover, the step segments themselves, and hence the impurities they interact with, are coarse-grained objects. Also, the above model is one sided, and does not account for contribution to the step velocity from the terrace behind. We do not expect a small contribution from the terrace behind to alter our conclusions. However, if the contribution is large, it can lead to a different instability of the Schwoebel type.[4] In Ref. 12, we studied such instabilities in the absence of impurities and found a very different behavior. The combination of the two types of instabilities may be of experimental relevance; we intend to investigate its consequences in the future.

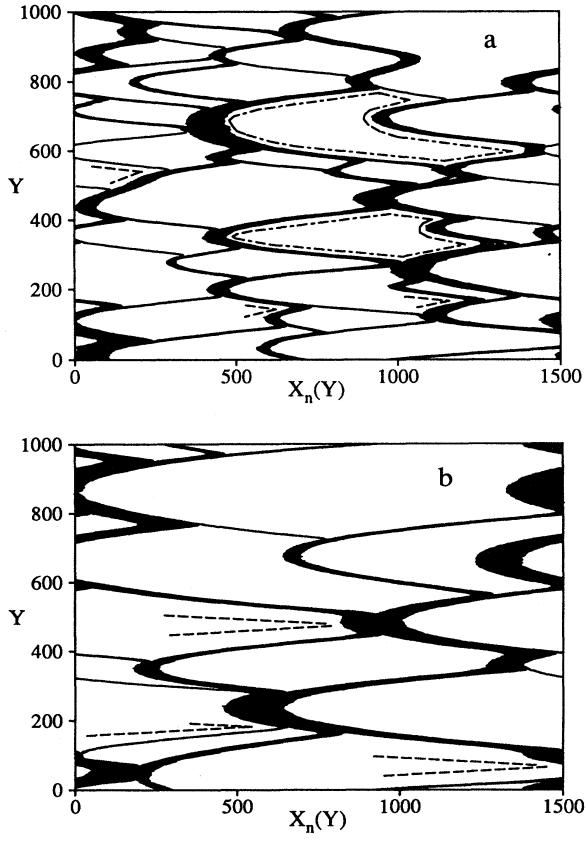

FIG. 1. (a) A typical step configuration after 30 000 Monte Carlo sweeps. The parameters are $l_d = 10$, $A = 0.9$, $\beta\gamma = 0.1$, $F_i = 0.005$, and $S = 0.65$. Vertices are marked by dashed lines, and dashed-dotted lines correspond to cells of the typical shape. (b) The same as (a) after 100 000 Monte Carlo sweeps. Here the dashed v-shaped lines denote the vertex shape obtained from the infinite period steady state.

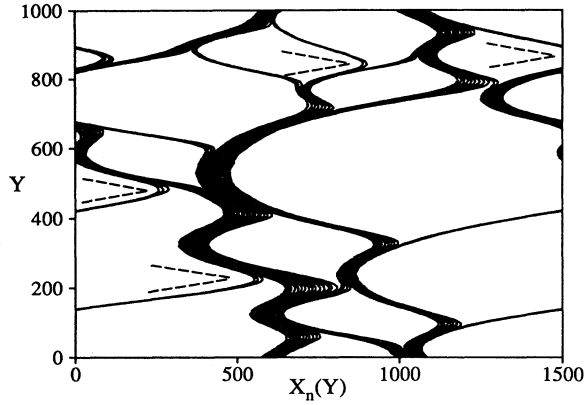

FIG. 2. A typical step configuration after 30 000 Monte Carlo sweeps. The parameters are $l_d = 10$, $A = 0.9$, $\beta\gamma = 1.0$, $F_i = 0.001$, and $S = 0.65$. The dashed v-shaped lines denote the vertex shape obtained from the infinite period steady state [Fig. 8(b)].

In Figs. 1, 2, and 3, we present typical step configurations of a system of $N = 30$ steps each consisting of $L = 1000$ segments, for different values of the line tension, impurity strength, and impurity flux parameters. Distances are measured in units of the lattice spacing, and time in Monte Carlo sweeps. The initial terrace width was $W^0 = 50$, and steps moved from left to right. We also used $l_d = 10$ and $A = 0.9$. Figure 1 is obtained from simulations with $\beta\gamma = 0.1$, $F_i = 0.005$, and $S = 0.65$ after 30 000 [Fig. 1(a)] and 100 000 [Fig. 1(b)] Monte Carlo sweeps. These complex highly connected step patterns indicate that step bending becomes very important in this model when the line tension is small, in contrast with the much simpler configurations obtained from simulations with large line tension (see Fig. 2 of Ref. 9), where the steps are basically straight.

We note that, in spite of the complexity of the patterns, they exhibit several simple repeating features.

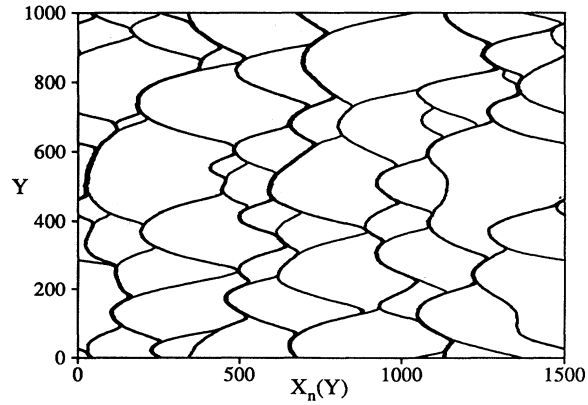

FIG. 3. A typical step configuration after 30 000 Monte Carlo sweeps. The parameters are $l_d = 10$, $A = 0.9$, $\beta\gamma = 1.0$, $F_i = 0.0005$, and $S = 0.95$.

(a) As in the large line tension case, there is a clear tendency of the steps to form bunches. The bunches are, in general, not straight. However, there are many straight bunch portions, which form a well defined angle, $\pm\alpha$, with respect to the original step orientation (parallel to the y axis).

(b) There are well-localized, pointlike regions at which a bunch of several steps splits into two smaller bunches. We call these points *vertices*. The portion of the bunch that approaches the vertex is typically straight and forms the angle $\alpha_1 = \pm\alpha$ with the y axis. One of the two smaller bunches that emerge from the vertex continues in the same direction of the original bunch, while the other turns around and goes in the other direction to form the angle $-\alpha_1$ with the y axis. Several vertices are marked as dashed lines in Fig. 1(a).

(c) The pattern divides the system into cells, many of which have the typical shape marked in Fig. 1(a) by dashed-dotted lines. It has a parabolic shape at its left side, a double-well-like shape at its right and two vertices one at the top and the other at the bottom.

As one can see from Fig. 1, these features do not have any noticeable time dependence. The pattern after 100 000 sweeps [Fig. 1(b)] is very similar to the one after 30 000 sweeps [Fig. 1(a)], except for a significant change in the typical length scale associated with the size of the cells. The length scale grows with time, but the angle α and the typical cell shape remain unchanged.

In Figs. 2 and 3 we show typical configurations for the parameters $\beta\gamma = 1.0$, $F_i = 0.001$, $S = 0.65$ and $\beta\gamma = 1.0$, $F_i = 0.0005$, and $S = 0.95$, respectively, after 30 000 Monte Carlo sweeps. Although the value of the angle α does depend on the parameters, the qualitative behavior of the system does not. Features (a)–(c) above, which we found in the patterns of Fig. 1, characterize Figs. 2 and 3 as well.

III. A DIFFERENTIAL EQUATION APPROACH

In order to understand the basic features of the step dynamics we described above, we now develop a simpler approach to the problem, which will then be analyzed analytically. First, consider the large line tension case. We showed in Ref. 9 that, as long as the impurities are not too strong (i.e., when $S \lesssim 0.69$), the kinetic model of Sec. II can be well approximated by an equation of the form (1), where f is given by a mean-field-like self-consistent equation in terms of S, F_i, and $f_0(W)$, the velocity function in the absence of impurities. In our case $f_0(W) \sim 1 - \exp(-W/l_d)$. We showed that as expected, $f(W)$ rises from zero at $W = 0$, reaches a maximum at some value of the terrace width, $W = W^m$, and then decreases exponentially to the constant $f(\infty) = f_0(\infty)(1 - S)$.

In Ref. 10 we generalized Eq. (1) to two dimensions, allowing for step fluctuations controlled by a line tension. Thus we replace (1) by the equation

$$\frac{\partial X_n(y)}{\partial t} = f[X_{n+1}(y) - X_n(y)] + \bar{\gamma}\frac{\partial^2 X_n(y)}{\partial y^2} + \eta_n(y). \tag{3}$$

Here y is a continuous coordinate normal to the x direction and $\bar{\gamma}$ is directly related to the step stiffness associated with step bending. ($1/\bar{\gamma}q^2$ is the relaxation time of fluctuations normal to the x direction along the step edge of wave number q.) η_n is a random uncorrelated noise term:

$$\begin{aligned} \langle \eta_n(y,t) \rangle &= 0, \\ \langle \eta_n(y,t)\eta_{n'}(y',t') \rangle &= 2\Gamma\delta_{n,n'}\delta(y-y')\delta(t-t'). \end{aligned} \tag{4}$$

In order to compare solutions of Eq. (3) with simulations of the model of the previous section, we need to determine the function $f(W)$ and the parameter $\bar{\gamma}$ that correspond to a particular set of parameters of the mesoscopic model. As we mentioned above, f can be determined from a mean-field theory as described in detail in Ref. 9. $\bar{\gamma}$ is calculated by measuring correlations of step fluctuations[13] in the absence of impurities. Thus, we carried out simulations of the mesoscopic model with the same values of the parameters that we used for investigating the instability, but with the flux of impurities $F_i = 0$. The uniform step train is completely stable in this case, and we observe simple stable flow of fairly straight, but fluctuating steps. We measure the correlation function

$$G(q,t) \equiv \frac{1}{L}\langle U_n(q,t')U_n(-q,t'+t)\rangle, \tag{5}$$

where

$$U_n(q,t) \equiv \sum_y \left[X_n(y,t) - \frac{1}{L}\sum_{y'} X_n(y',t) \right] e^{iqy} \tag{6}$$

is the Fourier transform of the step fluctuation amplitude. The angular brackets in Eq. (5) denote averaging over the step index n and over t'.

The correlation function $G(q,t)$ can also be calculated analytically from a discrete version of Eq. (3), where the second derivative term is replaced by $\bar{\gamma}[X_n(y+a) - 2X_n(y) + X_n(y-a)]$, with a being the lattice constant ($a = 1$ in the mesoscopic model). For large enough terrace width, the velocity function f_0 can be linearized around W^0 since the step fluctuation amplitude is small compared to the terrace width. Moreover, since f_0 approaches a constant exponentially, its derivative is exponentially small, and the only significant contribution of this term comes from $f_0(W^0)$. Under these approximations we obtain the following expression for $G(q,t)$:

$$G(q,t) = \frac{\Gamma \exp\{-2\bar{\gamma}[1-\cos(qa)]|t|\}}{2\bar{\gamma}[1-\cos(qa)]}. \tag{7}$$

Figure 4 is a logarithmic plot of $G(q,t)[1-\cos(qa)]$ as a function of $t[1-\cos(qa)]$ as obtained from simulations of the mesoscopic model with $\beta\gamma = 0.1$. When q is not too small, the data points fall on a straight line, confirming the validity of Eq. (7). For very small q our results are not reliable, since the relaxation time of fluctuations of wave number q diverges as $q \to 0$; therefore, one would have to simulate the system for exceedingly long times in order to obtain good accuracy for small q. From the straight line drawn in Fig. 4, we deduce that $\bar{\gamma} = 0.062$

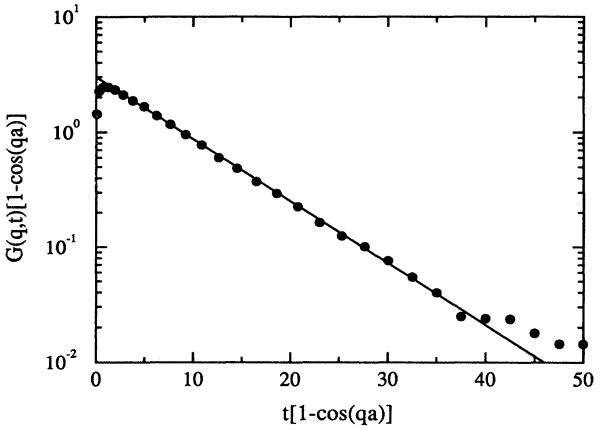

FIG. 4. A logarithmic plot of $G(q,t)[1-\cos(qa)]$ as a function of $t[1-\cos(qa)]$ for $\beta\gamma = 0.1$. The straight line corresponds to $\beta\bar{\gamma} = 0.062$ and $\Gamma = 0.37$. (See text for definitions.)

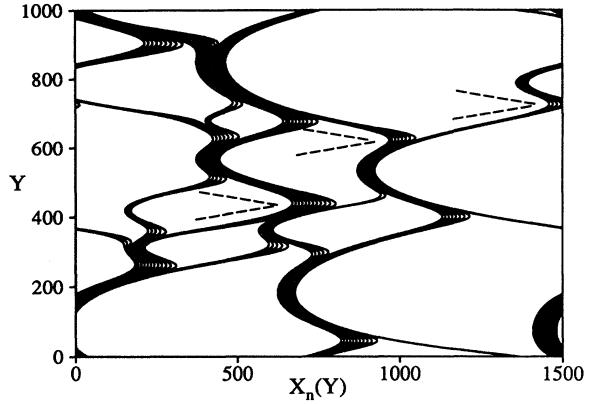

FIG. 6. A snapshot of a step system evolving according to Eq. (3). The function f came out of a mean-field calculation (Ref. 9) with the parameters of Fig. 2. We used $\bar{\gamma} = 0.4$ and $\Gamma = 0.16$. The vertex structure of the infinite period steady state is shown by v-shaped dashed lines.

and $\Gamma = 0.37$. We repeated this procedure for each set of mesoscopic parameters we used, in order to be able to compare with results from the analysis of the differential equation (3).

For example, we let the system evolve for some time according to Eq. (3) (starting from a uniform step train configuration) with the velocity function f obtained from the mean-field theory of Ref. 9 for the parameters $\beta\gamma = 0.1$, $S = 0.65$, $F_i = 0.005$, $l_d = 10$, and $A = 0.9$. We also used $\bar{\gamma} = 0.062$ and $\Gamma = 0.37$. Figure 5 is a typical configuration that results from this numerical solution. The resemblance to the configuration of Fig. 1(a) gives us confidence that the description in terms of the differential equation (3) is indeed satisfactory. To challenge the quantitative resemblance of the two approaches, we solved (3) once again, but with f that corresponds to $\beta\gamma = 1.0$ and $F_i = 0.001$ (the rest of the parameters remaining unchanged). Here we used $\bar{\gamma} = 0.4$ and $\Gamma = 0.16$

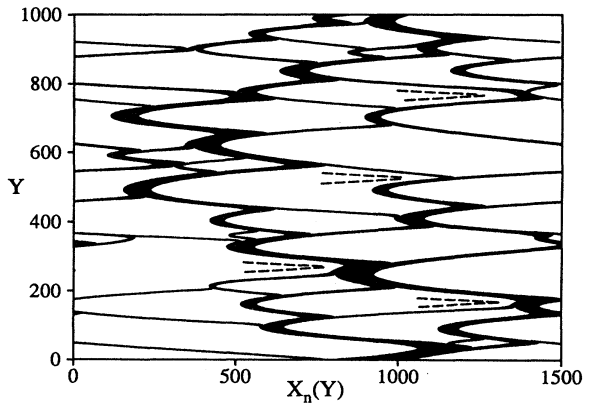

FIG. 5. A snapshot of a step system evolving according to Eq. (3). The function f came out of a mean-field calculation (Ref. 9) with the parameters of Fig. 1(a). We used $\bar{\gamma} = 0.062$ and $\Gamma = 0.37$. The vertex structure of the infinite period steady state is shown by v-shaped dashed lines.

as deduced for this case using the procedure described above (see Fig. 4). A resulting typical configuration is plotted in Fig. 6 and should be compared with Fig. 2. Again there is a qualitative as well as a quantitative similarity. We therefore conclude that the simpler description in terms of a differential equation combined with the mean-field theory of Ref. 9 and the procedure of finding $\bar{\gamma}$ outlined above is adequate and accurate. We now aim at understanding the kinetics that result from Eq. (3).

IV. STEADY STATES: ANALYTICAL SOLUTION FOR THE GENERAL PERIOD-TWO CASE

We do not know how to solve Eq. (3) in general. However, we can find special *steady-state* solutions which, as we show below, are relevant for the actual evolution of the system that results from the numerical solution of the equation. First, we will assume that it is sufficient to find steady states of (3) in order to understand the features of the patterns that do not depend strongly on time, such as the typical angle α, the typical cell shape, and the existence of vertices. This is a nontrivial assumption, since we know from simulations that the system keeps evolving and coarsening even after the features mentioned above become steady. This means that those steady states that are relevant for the evolution cannot be stable. On the other hand, they cannot be strongly unstable, since then the system would never come close to them. Therefore, we assume that our system is always locally close to *weakly unstable steady states*. The word "locally" here means that local features of the patterns can be deduced from steady states.

Our second assumption is that it is sufficient to look at steady states that have *period two* in the step index:

$$W_n(y,t) + W_{n+1}(y,t) = 2\tilde{W}, \tag{8}$$

where $\tilde{W}$ is independent of n, y, or t. This restriction is

less limiting than it might at first seem, since we intend to investigate only local properties of the patterns. Also, since the terrace behind does not affect step motion in our model, the evolution of a bunch is essentially determined by the kinetics of its leading step (with the highest step index), while the rest of the steps in the bunch follow it. Therefore, a bunch of steps behaves like a single step, except at vertices where there is bunch splitting. A pair, or a bunch of two steps, is sufficient to describe a vertex, since we rarely see splitting into more than two bunches. Lastly, we note that in the absence of noise, if Eq. (8) is satisfied at $t = 0$, it is satisfied for any $t > 0$, which makes condition (8) consistent with the evolution equation (3). These arguments make the pair assumption reasonable, but ultimately a comparison of the structures obtained with results from simulations will determine its validity. For now, our goal is to find all the steady states of (3) (without noise) that satisfy the period-two restriction (8).

In the absence of noise, Eq. (3) takes the form

$$\frac{\partial W_n(y)}{\partial t} = f[2\tilde{W} - W_n(y)] - f[W_n(y)] + \bar{\gamma}\frac{\partial^2 W_n(y)}{\partial y^2}, \tag{9}$$

where we used restriction (8), thus replacing the infinite set of coupled equations (3) by a single equation for one unknown function. Setting the left-hand side of (9) to zero, we obtain the steady-state equation

$$\bar{\gamma}\frac{d^2 W_n^s}{dy^2} = -\frac{dV}{dW_n^s}, \tag{10}$$

where $W_n^s(y)$ is the steady-state terrace width, and V has the form

$$V(W_n^s) \equiv \int^{W_n^s} \left[f(2\tilde{W} - W) - f(W)\right] dW. \tag{11}$$

Thus, we have transformed the steady-state problem to an equation of motion for a classical particle of mass $\bar{\gamma}$ moving in the potential V. W_n^s corresponds to the position of the particle, and y is analogous to time. V is obviously symmetric around $W_n^s = \tilde{W}$.

We are interested in all the possible trajectories of the particle that are bounded in the interval $0 < W_n^s < 2\tilde{W}$. The lower bound condition accounts for the no-overhang condition, or the fact that f is undefined for $W < 0$. The trajectory of the particle (or equivalently the terrace width as a function of y) depends on the form of the potential V, which in turn depends on the value of the average terrace width $\tilde{W}$. Consider the two possibilities $\tilde{W} < W^m$ and $\tilde{W} > W^m$. In both cases we can obtain the shape of the potential from our knowledge of the general shape of the velocity function f, which rises from zero near $W = 0$, reaches a maximum at $W = W^m$, and decreases to a constant for $W > W^m$. We plotted schematically the shape of V for $\tilde{W} < W^m$ in Fig. 7(a) and for $\tilde{W} > W^m$ in Fig. 7(b). In the first case V has a single maximum at $W_n^s = \tilde{W}$, and as a result the only possible trajectory confined in the interval $0 < W_n^s < 2\tilde{W}$ is $W_n^s(y) = \tilde{W}$ for any y. This is of course the uniform step train solution with straight steps. We expect (see Sec. I) this uniform step system to be stable with respect to the kinetics given by Eq. (9), as is indeed verified by the linear stability analysis of Sec. VIII.

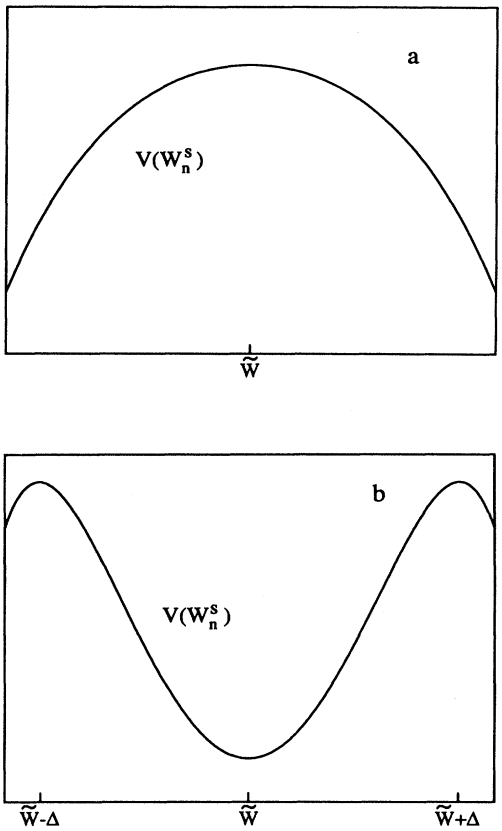

FIG. 7. A schematic plot of the Newtonian potential [Eq. (11)] for (a) $\tilde{W} < W^m$ and (b) $\tilde{W} > W^m$.

A more interesting case arises when $\tilde{W} > W^m$. The potential then has a minimum at $W_n^s = \tilde{W}$ [Fig. 7(b)], but also has two maxima at $W_n^s = \tilde{W} \pm \Delta$, where $\Delta < \tilde{W}$ depends on the velocity function f. Now there are two kinds of solutions. First, there are three solutions that correspond to straight steps: the uniform step train $W_n^s(y) = \tilde{W}$, and the two equivalent pair solutions $W_n^s(y) = \tilde{W} \pm \Delta$. The uniform step train is unstable in this case (see Sec. VIII), and the two paired states are irrelevant for the small line tension kinetics except perhaps as a limiting case of $t \to \infty$ in a finite system. Indeed, straight step configurations are not observed throughout the simulation.

Solutions of the second kind, where the steps are not straight, are the most interesting ones, and as we show below, are also the most relevant ones for the kinetics of our step patterns. There is a continuous family of such solutions, and they are all periodic in "time" (the y coordinate). They are bounded in the interval $\tilde{W} - \Delta < W_n^s < \tilde{W} + \Delta$, and are characterized by one parameter: the integral of the motion of Eq. (10), i.e., the "energy" of the Newtonian particle

$$\mathcal{E} = \frac{1}{2}\bar{\gamma}\left(\frac{dW_n^s}{dy}\right)^2 + V[W_n^s(y)]. \quad (12)$$

$\mathcal{E}$ is independent of y and can take any value between $V(\tilde{W})$ and $V(\tilde{W}+\Delta)$. Each solution in the family has two extremal points, $W^{\pm}(\mathcal{E})$ (with $W^+ > W^-$ and $W^+ + W^- = 2\tilde{W}$) at which the particle has no "kinetic energy", i.e., $V(W^{\pm}) = \mathcal{E}$. In each period of its motion, the particle visits each of the extremal point once with vanishing "velocity," while the maximal velocity is achieved at the minimum of the potential ($W_n^s = \tilde{W}$), which is visited twice in a period. The period of the motion [and hence the period of $W_n^s(y)$], $l(\mathcal{E})$, can be obtained by integrating expression (12) for y from $\tilde{W}$ to W^+:

$$l(\mathcal{E}) = 4\sqrt{\frac{\bar{\gamma}}{2}}\int_{\tilde{W}}^{W^+}\frac{dW}{\sqrt{\mathcal{E}-V(W)}}. \quad (13)$$

The above analysis is a complete characterization of all the steady states of Eq. (9) for any velocity function f with the general form assumed in the Introduction. In the next section we will show that these steady-state solutions explain all the three repeating features we found in the step patterns of Figs. 1–3.

V. COMPARISON WITH SIMULATIONS

A vertex where a pair of steps splits in two corresponds to the times when W_n^s visits the minimum of the potential at $\tilde{W}$. The fact that the kinetic energy of the particle is maximal at the potential minimum implies that it stays there only a short "time," which explains why the vertices in the patterns are so well localized in a small region of space. The angle α can be understood by considering steady-state solutions with very large periods, which should be relevant for the long time behavior of the system (see Sec. VIII). As we demonstrate below, the function $X_n(y)$ that corresponds to these solutions is fairly straight over long distances between vertices. These straight portions form a well defined angle with the y axis. In particular, there is one infinite period steady state that corresponds to the energy $\mathcal{E} = V(\tilde{W}+\Delta)$, where $l(\mathcal{E})$ diverges [see Eq. (13)]. This is a single vertex solution that approaches a straight line far from the vertex. The asymptotic angle associated with this straight line is α.

In order to be more quantitative, we solved the steady-state equation (10) numerically for the velocity functions and the values of $\bar{\gamma}$ that correspond to the patterns of Fig. 2. By starting from different initial configurations, we were able to find several steady states with different periodicities in y. From the knowledge of $W_n^s(y)$, we can find $X_n(y,t) = X_n^s(y) + vt$ by solving the differential equation [see Eq.(3)]

$$v = f[W_n^s(y)] + \bar{\gamma}\frac{d^2X_n^s(y)}{dy^2} \quad (14)$$

for $X_n^s(y)$. Boundary conditions fix the integration constants, but how is the steady-state step velocity v determined? In principle, there is a solution for any value of v. Generically, however, the solution for X_n^s diverges as $y \to \infty$ because of the term quadratic in y, which is produced by integrating f twice with respect to y. This term can only be canceled by choosing the value of v properly. Thus, there is only one allowed value of v for a given $W_n^s(y)$ if we do not allow divergences. See the discussion in Sec. VII below for an explicit example.

In Figs. 8(a) and 8(b) we show two of the configurations that correspond to steady states we found numerically. Figure 8(a) is a steady state with a finite period in the y direction. Although it is more ordered than the patterns of Figs. 1 and 2, the similarity in the local features is evident. The steady-state solution contains vertices, as well as straight portions of bunches (pairs of steps in this case) that form a well defined angle with the y axis. Even the typical cell shape of the steady state is strikingly similar to the one marked by dashed-dotted lines in Fig. 1(a). Figure 8(b) is the single vertex infinite period solution, from which we can clearly get an estimate of the angle α. The dashed v-shaped lines in Figs. 2 and 6 mark the angles $\pm\alpha$ of the infinite period steady state as measured from Fig. 8(b). There is clearly a quantitative agreement between this calculation, Monte Carlo simulations (Fig. 2), and the numerical solution of the differential equation

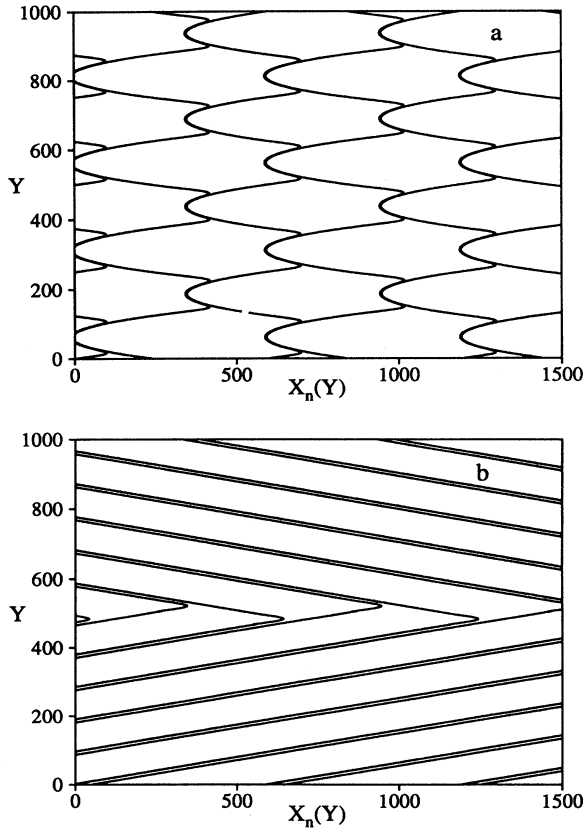

FIG. 8. (a) A finite period steady state calculated for the function f of Fig. 2 and $\bar{\gamma} = 0.4$. (b) The infinite period steady state.

(3). A similar comparison can be found in Figs. 1(b) and 5, where the angles marked by the v-shaped lines are the infinite period steady-state angles calculated with the velocity function f and $\bar{\gamma}$ that correspond to the patterns of the two figures. Again the agreement is very impressive. In fact, it is better than what one might expect keeping in mind the approximations that we made.

VI. CLOSED FORM SOLUTION: CASE A

In this section and the next one we show that for certain forms of the function f, we can express some of the steady states in closed analytic form. It is not easy to come up with a velocity function for which Eq. (10) can be solved exactly. One possible strategy is to start from a given function $X_n^s(y)$ that has the features of the steady-state solutions described in Sec. IV, and then work backwards to find the associated velocity function f for which that $X_n^s(y)$ solves Eq. (10). The single vertex steady-state solution (with an infinite period) of Fig. 8(b) has a particularly simple form and seems a good place to start. Requiring that the terrace width $W_n^s(y)$ approaches its asymptotic values $\tilde{W} \pm \Delta$ exponentially fast as $y \to \pm\infty$ led us to consider the functional form

$$X_n^s(y) = n\tilde{W} - \lambda \ln\cosh\left[\frac{y}{\lambda}\tan\alpha + (-)^n\frac{\Delta}{2\lambda}\right], \quad (15)$$

where λ is a new length parameter, $\tilde{W}$ is the average terrace width as defined in Sec. IV, and α is the angle the straight bunch portions form with the y axis. Recall that Δ was defined such that, for $\tilde{W} > W^m$, the potential V has two maxima at $W_n^s = \tilde{W} \pm \Delta$. The idea is now to find the appropriate f for which $X_n^s(y)$ in (15) is an exact solution when a proper choice of the parameters in (15) is made. We can do this by solving the following equation for f:

$$v = f[W_n^s(y)] + \bar{\gamma}\frac{d^2X_n^s(y)}{dy^2} = f(\tilde{W}+\Delta) = f(\tilde{W}-\Delta), \quad (16)$$

where we used Eq. (14) together with the fact that $d^2X_n^s/dy^2 \to 0$ as $y \to \pm\infty$ [from Eq. (15)].

Using Eq. (15) and hyperbolic identities, we can find expressions for $W_n^s(y)$:

$$W_n^s(y) = \tilde{W} - \lambda\ln\cosh\frac{\Delta}{\lambda} - \lambda\ln\left[1 - (-)^n\tanh\frac{\Delta}{\lambda} \times \tanh\left(\frac{y}{\lambda}\tan\alpha + (-)^n\frac{\Delta}{2\lambda}\right)\right] \quad (17)$$

and for $d^2X_n^s/dy^2$

$$\frac{d^2X_n^s}{dy^2} = -\frac{\tan^2\alpha}{\lambda}\left[1 - \tanh^2\left(\frac{y}{\lambda}\tan\alpha + (-)^n\frac{\Delta}{2\lambda}\right)\right]. \quad (18)$$

The only y dependence is contained in the factor $\tanh\left[\frac{y}{\lambda}\tan\alpha + (-)^n\frac{\Delta}{2\lambda}\right]$, which is common to both (17) and (18). This means that we can solve for $d^2X_n^s/dy^2$ in terms of W_n^s, and hence directly determine $f(W_n^s)$ from (16).

To isolate that common factor in (17), it is convenient first to define W^m such that

$$e^{-W^m/\lambda} \equiv e^{-\tilde{W}/\lambda}\cosh\frac{\Delta}{\lambda}. \quad (19)$$

We will see later that the resulting function f indeed has a maximum at W^m. We therefore fix the value of W^m, and Eq. (19) becomes an expression for Δ in terms of $\tilde{W}$. For each $\tilde{W} > W^m$ there is a unique solution of (19) with $\Delta > 0$.

Combining this definition of W^m with Eq. (17), we arrive at the following equation:

$$\tanh^2\frac{\Delta}{\lambda}\tanh^2\left(\frac{y}{\lambda}\tan\alpha + (-)^n\frac{\Delta}{2\lambda}\right) = E(W_n^s(y)), \quad (20)$$

where we define

$$E(W) \equiv \left[1 - \exp\left(-\frac{W-W^m}{\lambda}\right)\right]^2. \quad (21)$$

Note that $E(W^m) = 0$ and $E(\infty) = 1$. From the limiting cases $y \to \pm\infty$, we get

$$\tanh^2\frac{\Delta}{\lambda} = E(\tilde{W}+\Delta) = E(\tilde{W}-\Delta), \quad (22)$$

which also follows directly from (19). Using the last three equations together with (18), we can express $d^2X_n^s/dy^2$ in terms of W_n^s:

$$\frac{d^2X_n^s}{dy^2} = -\frac{\tan^2\alpha}{\lambda}\left(1 - \frac{E(W_n^s)}{E(\tilde{W}+\Delta)}\right). \quad (23)$$

Inserting expression (23) in Eq. (16), we get the function $f(W_n^s)$:

$$f(W_n^s) = f(\tilde{W}+\Delta) + \frac{\bar{\gamma}}{\lambda}\tan^2\alpha\left(1 - \frac{E(W_n^s)}{E(\tilde{W}+\Delta)}\right), \quad (24)$$

and now it becomes obvious that $f(W_n^s)$ reaches its maximum at W^m. Expression (24) can be simplified further. For $W_n^s = W^m$, we have

$$\frac{\bar{\gamma}}{\lambda}\tan^2\alpha = f(W^m) - f(\tilde{W}+\Delta), \quad (25)$$

and Eq. (24) becomes

$$f(W_n^s) = f(\tilde{W}+\Delta) + [f(W^m) - f(\tilde{W}+\Delta)]\left(1 - \frac{E(W_n^s)}{E(\tilde{W}+\Delta)}\right). \quad (26)$$

Note that the function f thus obtained depends, in prin-

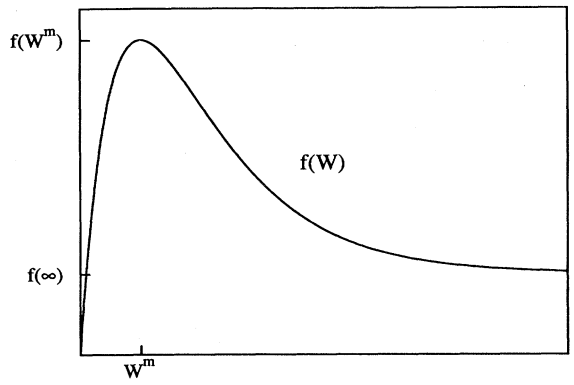

FIG. 9. A schematic plot of the velocity function $f(W)$ that corresponds to Eq. (28). The function plotted corresponds to $W^m/\lambda = 0.77$, and therefore $f(W^m)/f(\infty) \approx 3.9$.

ciple, on $\tilde{W}$. However, for the particular choice of X_n^s in Eq. (15), there is no such dependence. This can be seen by rewriting Eq. (26) in the following way:

$$[f(W_n^s) - f(W^m)]\,/\,E(W_n^s) = [f(\tilde{W}+\Delta) - f(W^m)]\,/\,E(\tilde{W}+\Delta)\,. \quad (27)$$

The equality of functional forms in (27) means that the expression on the left-hand side equals a constant C that does not depend on the value of W_n^s or on the value of $\tilde{W}+\Delta$. We can choose C such that the no-crossing condition $f(0)=0$ is satisfied. (A finite minimal distance is treated similarly.) This yields our final result

$$f(W) = f(W^m)\left[1 - \frac{E(W)}{E(0)}\right]. \quad (28)$$

A necessary condition for a physically acceptable velocity function is that $f(\infty) \geq 0$. This requires $E(0) \geq 1$, or $W^m/\lambda \geq \ln 2$.

Thus, we get the function that is drawn schematically in Fig. 9. As expected, it increases linearly from $f(0)=0$ for small W, has a maximum at W^m, and decreases exponentially to $f(\infty)$ with a decay constant λ. For this function we know the *exact* infinite period solution, Eq. (15); this method gives us no information about the finite period solutions associated with (28). From (25) the angle α satisfies the equation

$$\tan^2\alpha = \frac{\lambda}{\bar{\gamma}} f(W^m)\frac{E(\tilde{W}+\Delta)}{E(0)}. \quad (29)$$

Note that for large $\tilde{W}$ (which is relevant for the long time behavior of the system of steps) the dependence of α on $\tilde{W}$ is very weak and can be ignored for all practical purposes.

VII. CLOSED FORM SOLUTION: CASE B

Another form of f for which we can solve the steady-state equation (10) exactly even for finite periods is

$$f(W) = aW - bW^2 + cW^3, \quad (30)$$

with $a,b,c>0$ and

$$\sqrt{\frac{27ac}{8}} < b < \sqrt{4ac}. \quad (31)$$

This function does not have the form assumed throughout this paper for all W. It reaches a maximum at $W^m = (b-\sqrt{b^2-3ac})/3c$, and a minimum at $W^\star = (b+\sqrt{b^2-3ac})/3c$, but for large W it is an increasing function of its argument. However, for the purpose of finding paired steady states we do not need to know f for $W > 2\tilde{W}$, and therefore if we choose

$$W^m < \tilde{W} < W^\star/2, \quad (32)$$

then f as defined in (30) has all the properties we need in modeling Frank's instability. Condition (31) guarantees that $W^\star/2 > W^m$ [in order to satisfy Eq. (32)] and $f(W^\star) > f(0) = 0$.

Now the potential V defined in Eq. (11) has (as before) a minimum at $W_n^s = \tilde{W}$ and two maxima at $W_n^s = \tilde{W}\pm\Delta$ with

$$\Delta = \sqrt{\tilde{W}^2 - \frac{a - 2b\tilde{W} + 4c\tilde{W}^2}{c}}. \quad (33)$$

Defining a new function $U(y) \equiv W_n^s(y) - \tilde{W}$, the steady-state equation (10) takes the form

$$\bar{\gamma}\frac{d^2U}{dy^2} = 2c(U^3 - U\Delta^2). \quad (34)$$

The solution of this equation is

$$U(y) = \bar{U}\,\mathrm{sn}\left[\frac{\mu}{\sqrt{\bar{\gamma}}}(y-y_0), k\right], \quad (35)$$

where sn is a Jacobian elliptic function, y_0 is an arbitrary real number, μ is a real number with the restriction $c\Delta^2 \leq \mu^2 \leq 2c\Delta^2$, and

$$k^2 = 2c\frac{\Delta^2}{\mu^2}, \quad \bar{U}^2 = 2\Delta^2 - \frac{\mu^2}{c}. \quad (36)$$

The potential is $V(U) = cU^2\Delta^2 - cU^4/2$ and the Newtonian energy is

$$\mathcal{E} = V(U) + \frac{1}{2}\bar{\gamma}\left(\frac{dU}{dy}\right)^2 = \frac{1}{2}\bar{U}^2\mu^2 \geq 0. \quad (37)$$

The period of the solution with parameter k is

$$l(k) = 4\int_0^{\frac{\pi}{2}} \frac{d\Phi}{\sqrt{1-k^2\sin^2\Phi}}. \quad (38)$$

The solutions (35) have all the properties described in Sec. IV for the general case. Here too we can use Eq. (14) to calculate $X_n^s(y)$ from our knowledge of $W_n^s(y)$. Let us demonstrate this procedure for the infinite period solution that corresponds to $k=1$:

$$W_n^s(y) = \tilde{W} \pm \Delta \tanh\left(\sqrt{\frac{c}{\bar{\gamma}}}\Delta y\right), \tag{39}$$

where we took $y_0 = 0$. Integrating Eq. (14) twice with respect to y we obtain the following expression for X_n^s:

$$\begin{aligned} X_n^s(y) = {} & \frac{1}{2\bar{\gamma}}[v - (a\tilde{W} - b\tilde{W}^2 + c\tilde{W}^3) - (3c\tilde{W} - b)\Delta^2]y^2 \\ & + \left(c_1 \pm \frac{1}{2\bar{\gamma}}c\Delta^2\sqrt{\frac{\bar{\gamma}}{c}}\right)y + c_2 \\ & - \frac{b - 3c\tilde{W}}{c}\ln\cosh\left(\sqrt{\frac{c}{\bar{\gamma}}}\Delta y\right) \\ & \mp \frac{1}{2}\Delta\tanh\left(\sqrt{\frac{c}{\bar{\gamma}}}\Delta y\right), \end{aligned} \tag{40}$$

where c_1 and c_2 are constants of integration. The value of v is determined from the requirement that the y^2 term vanish, and c_1 is chosen so that the term linear in y vanishes too. The pair infinite period solution now becomes

$$\begin{aligned} X_n^s(y) = {} & n\tilde{W} - \frac{b - 3c\tilde{W}}{c}\ln\cosh\left(\sqrt{\frac{c}{\bar{\gamma}}}\Delta y\right) \\ & + (-)^n\frac{\Delta}{2}\tanh\left(\sqrt{\frac{c}{\bar{\gamma}}}\Delta y\right) \end{aligned} \tag{41}$$

and the angle α is

$$\tan\alpha = \frac{b - 3c\tilde{W}}{c}\sqrt{\frac{c}{\bar{\gamma}}}\Delta. \tag{42}$$

VIII. STABILITY AND COARSENING KINETICS

In this section we support our main assumption (see Sec. IV) that the system of steps is always locally close to *weakly unstable steady states*, by showing that the steady states we calculated in Secs. IV, VI, and VII are indeed weakly unstable. To that end we carry out a linear stability analysis of Eq. (9) around the steady-state solutions $W_n^s(y)$. By setting $W_n(y,t) = W_n^s(y) + \delta W_n(y,t)$ and expanding (9) to linear order in δW_n, we obtain the following equation:

$$\frac{\partial \delta W_n}{\partial t} = -\left[f'(2\tilde{W} - W_n^s) + f'(W_n^s)\right]\delta W_n + \bar{\gamma}\frac{\partial^2 \delta W_n}{\partial y^2}, \tag{43}$$

where f' is the derivative of f. We can separate the variables in this equation. Thus, if $\delta W_n(y,t) \equiv g(y)h(t)$, the solution for h is $h(t) \sim \exp(\omega t)$, and the function g obeys the equation

$$-\bar{\gamma}\frac{d^2 g}{dy^2} - \frac{d^2 V}{d(W_n^s)^2}g = -\omega g. \tag{44}$$

This is a Schrödinger equation for the wave function g describing a quantum mechanical particle moving in the periodic potential $-d^2V/d(W_n^s)^2$.

In order to determine the stability of the steady-state W_n^s, we have to calculate the most unstable perturbation, which corresponds to the ground state of the Schrödinger equation with energy $-\omega^{\max}$. After rewriting (14) in terms of W_n^s, it is easy to see by direct substitution that dW_n^s/dy is an eigenfunction of (44) with eigenvalue $\omega = 0$. Therefore each steady state has a marginal perturbation, and $\omega^{\max}$ is bounded from below by zero. Now consider the steady state, $W_n^s(y) = \tilde{W}$, which corresponds to the lowest value of $\mathcal{E}$. In this case the quantum mechanical potential is independent of y and the Schrödinger equation can be solved exactly. As expected, the ground state energy here is negative and this steady state is unstable with positive $\omega^{\max} = d^2V/dW_n^s$ evaluated at $W_n^s = \tilde{W}$. We know already that $\omega^{\max}$ does not become negative for any value of $\mathcal{E}$ (since it is bounded from below by zero), and assuming that $\omega^{\max}(\mathcal{E})$ is an analytic function, we conclude that $\omega^{\max} > 0$ for any $\mathcal{E} < V(\tilde{W} + \Delta)$. Thus all the periodic steady states are unstable. We still have to show that they are only *weakly* unstable.

We are interested in the limit of large terrace width $\tilde{W}$, and will carry out a simple scaling analysis of Eq. (44) to find out how $\omega^{\max}$ behaves in this limit. To that end we assume that $\tilde{W}$ is the only length scale in the system. Consistently, the expression for the period l has the form

$$l = 4\sqrt{\frac{\bar{\gamma}}{2}}\tilde{W}\int_1^{R^+}\frac{dR}{\sqrt{\mathcal{E} - V}}, \tag{45}$$

where $R = W/\tilde{W}$ and $R^+ = W^+/\tilde{W}$. With the definitions $R_n^s \equiv W_n^s/\tilde{W}$ and $\bar{y} \equiv y/\tilde{W}$, Eq. (44) takes the form

$$-\bar{\gamma}\frac{d^2 g}{d\bar{y}^2} - \frac{d^2 V}{d(R_n^s)^2}g = -\omega^{\max}\tilde{W}^2 g, \tag{46}$$

from which we conclude that $\omega^{\max} \sim \tilde{W}^{-2}$. Therefore, $\omega^{\max}$ is very small in the large $\tilde{W}$ limit, which confirms our assumption that the long period steady states are

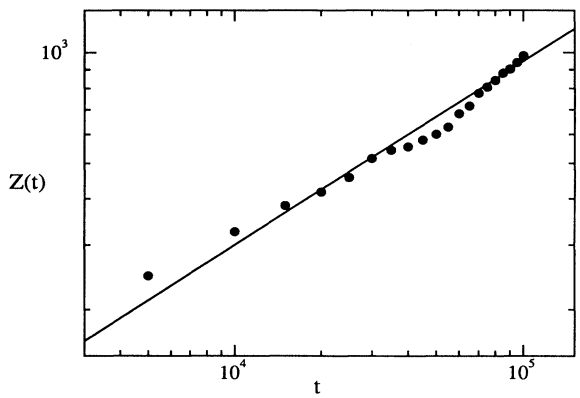

FIG. 10. The average cell size, Z, as a function of time as obtained from numerical simulations of the mesoscopic model. The solid line corresponds to $Z = 3\sqrt{t}$.

weakly unstable.

This analysis also allows us to calculate the asymptotic divergence of the typical length scale of the system (e.g., the cell size) with time. Assuming the time scale associated with the coarsening behaves as $1/\omega^{\max}$, we obtain the coarsening law

$$l \sim \tilde{W} \sim t^{1/2}. \tag{47}$$

In Fig. 10 we plotted the average cell size, Z, as a function of time, calculated from patterns that were obtained from numerical simulations of the mesoscopic model (see Fig. 1). The solid line corresponds to the function $Z = 3t^{1/2}$. Thus, the numerical results are consistent with the theoretical prediction, but more extensive simulations are needed in order to achieve a more stringent test of the theory.

IX. SUMMARY

We have proposed both a mesoscopic model and a differential equation approach to study the effect of impurities on the morphology of crystal surfaces during growth and evaporation in the step flow mode. The two models lead to quantitatively similar patterns of steps. These patterns, although highly connected and extremely complex, have several simple repeating features. The simple features do not depend on time although the typical length scale associated with the patterns does grow.

In order to explain the repeating time-independent features, we made the ansatz that the system is locally close to weakly unstable steady states. We found (analytically) a continuous family of steady states of the differential equation model, and showed that they have all the local features of the patterns generated by simulations. Moreover, the agreement between the steady states and the time-dependent patterns is quantitative, thus verifying the validity of our ansatz.

A linear stability analysis of the differential equation around the steady states showed that those states whose typical length scale is very long are indeed weakly unstable. Also, we predicted that the typical length scale should grow as $\sqrt{t}$, in agreement with numerical simulations of the mesoscopic model.

We are not aware of careful experiments aimed at studying impurity induced step patterns. Our study of impurity induced effects yielded very detailed qualitative as well as quantitative predictions, which can be easily compared with experiments. We therefore hope that our effort will lead to experimental searches for the phenomena we discussed and to possible tests of the ideas advanced in this work.

ACKNOWLEDGMENTS

We thank N. C. Bartelt, M. E. Fisher, E. D. Williams, and Y.-N. Yang for stimulating discussions. This work was supported in part by the National Science Foundation under Grant No. NSF-DMR-91-03031.

---

* Present address: Gordon McKay Laboratory, Harvard University, 9 Oxford St., Cambridge, MA 02138.

[1] W. K. Burton, N. Cabrera, and F. C. Frank, Philos. Trans. R. Soc. London Ser. A **243**, 299 (1951).

[2] P. M. Petroff, A. C. Gossard, and W. Wiegmann, Appl. Phys. Lett. **45**, 620 (1984); M. S. Miller, H. Weman, C. E. Pryor, M. Krishnamarthy, P. M. Petroff, H. Kroemer, and J. L. Merz, Phys. Rev. Lett. **68**, 3464 (1992).

[3] See, for example, J. Bloem and L. J. Giling, Curr. Top. Mater. Sci. **1**, 147 (1978); W. J. P. van Enckevort, Prog. Cryst. Growth Charact. **9**, 1 (1984); A. V. Latyshev, A. L. Aseev, A. B. Krasilnikov, and S. I. Stenin, Surf. Sci. **213**, 157 (1989).

[4] R. L. Schwoebel and E. J. Shipsey, J. Appl. Phys. **37**, 3682 (1966); R. L. Schwoebel, *ibid.* **40**, 614 (1969).

[5] G. S. Bales and A. Zangwill, Phys. Rev. B **41**, 5500 (1990).

[6] F. C. Frank, in *Growth and Perfection of Crystals*, edited by R. Doremus, B. Roberts, and D. Turnbull (Wiley, New York, 1958), p. 411; see also N. Cabrera and D. A. Vermilyea, *ibid.*, p. 393.

[7] J. P. v. d. Eerden and H. Muller-Krumbhaar, Phys. Rev. Lett. **57**, 2431 (1986); Phys. Scr. **40**, 337 (1989).

[8] D. Kandel and J. D. Weeks, Phys. Rev. Lett. **69**, 3758 (1992); Physica D **66**, 78 (1993).

[9] D. Kandel and J. D. Weeks, Phys. Rev. B **49**, 5554 (1994).

[10] D. Kandel and J. D. Weeks, Phys. Rev. Lett. **72**, 1678 (1994).

[11] P. Bennema and G. H. Gilmer, in *Crystal Growth: An Introduction*, edited by P. Hartman (North-Holland, Amsterdam, 1973), p. 263.

[12] D. Kandel and J. D. Weeks, Phys. Rev. Lett. **74**, 3632 (1995).

[13] N. C. Bartelt, J. L. Goldberg, T. L. Einstein, E. D. Williams, J. C. Heyraud, and J. J. Métois, Phys. Rev. B **48**, 15 453 (1993).